Measurement and Simulation of Sooting Characteristics by an ATJ-SKA Biojet Fuel and Blends with Jet A-1 fuel in Laminar Diffusion Flames

Bo Tian[a,b], Anxiong Liu[c,d] , Cheng Tung Chong[e*], Luming Fan[a], Shiyao Ni[a], Andrew Hull[f], Angelica Hull[f], Stelios Rigopoulos[d], Kai Luo[c], Simone Hochgreb[a]

[a] *Department of Engineering, University of Cambridge, Trumpington Street, CB2 1PZ Cambridge, UK*
[b] *College of Engineering and Technology, University of Derby, Markeaton Street, DE22 3AW Derby, UK*
[c] *Department of Mechanical Engineering, University College London, Torrington Place, London WC1E 7JE, UK*
[d] *Department of Mechanical Engineering, Imperial College London, South Kensington Campus, London SW7 2AZ, UK*
[e] *China-UK Low Carbon College, Shanghai Jiao Tong University, Lingang, Shanghai 201306, China*
[f] *Swedish Biofuels AB, Fjällvägen 3, 181 31 Lidingö, Sweden*

Abstract

We investigate the sooting propensity of an Alcohol-to-Jet-Synthetic Kerosene with Aromatics (ATJ-SKA) biojet fuel. The soot volume fraction and primary particle size in the pre-vaporised diffusion flames using ATJ-SKA biojet and blends with Jet A-1 at atmospheric conditions were measured experimentally and compared to numerical simulations. The measurements were conducted using extinction calibrated laser induced incandescence (LII). Within the 10% measurement uncertainty, the soot volume fractions measured using ATJ-SKA fuel do not show significant difference with measurements with Jet A-1. A comparison of the chemical composition of the fuels suggests that the Degree of Unsaturation (DoU) may not determine the sooting propensity of biojet fuels. The SEM analysis shows that diffusion flames using neat Jet A-1 produce finer soot particles and larger number density of compared to biojet and biojet surrogate. The soot model employs a semi-detailed chemical kinetic mechanism and a physical model which integrates the population balance equation governing the soot particle size distribution with the in-house reactive flow solver for multicomponent ideal gases. The model predicted the soot maximum soot volume fraction (SVF_m) in the neat biojet case and the blended cases with Jet A-1 fuels within an error margin of 13% comparing with the measured values. However, the predicted a soot volume fraction distribution patterns differ with the measured ones and the possible reasons are discussed.

Key words : Biojet fuel; Soot; Laser induced incandescence (LII); Diffusion flame

* Corresponding author: C T Chong (ctchong@sjtu.edu.cn) B Tian (b.tian@derby.ac.uk)

1. Introduction

The aviation industry is expected to grow over the next two decades in tandem with the growing population [1]. Passenger and cargo traffic for aviation industry is forecast to grow at the rate of 5% per annum until 2034 [2], while the International Air Transport Association (IATA) has projected an increase of air-travel passengers to 7.2 billion by 2035 [3]. The increase in travel will inevitably consume more aviation fuels and will in turn lead to an increase in pollutant emissions and greenhouse gases. The release of fine particles from the aircraft engine, commonly known as particulate matter (PM), has been a subject of scientific investigation owing to its impact on the upper atmosphere [4] and local air quality near airports [5]. Biomass-derived jet fuels, also known as biojet fuels, have gained much attention in recent years owing to sustainability and the potential of GHG reductions [6,7]. It is expected that the uptake of biojet fuel will continue to grow in the near future, in response to the decarbonization target set by IATA and the aviation community to reduce GHG by 50% (relative to 2005 level) by 2050 for the aviation sector, where a substantial portion of GHG reduction is to be achieved via the adoption of biojet fuel [1]. The ultimate goal of reducing GHG and pollutant emissions has spurred the development of biojet fuel via different production pathways and feedstocks, hence detailed understanding of the fuel chemistry and pollutant formation mechanism becomes important.

Evaluation of the sooting propensity of alternative jet fuels in real jet engines has been performed by various research groups [8,9]. In a CFM56-7B engine test simulating the landing and take-off cycle, Lobo *et al.* [9] showed a reduction of 62% of PM emissions was achieved for the neat FT fuel compared to the Jet A-1 fuel. The reduction of PM emissions was attributed to the absence of aromatics content in FT fuel, as opposed to the 18.5 vol% of aromatics in the Jet A-1. Although lower aromatics content in synthetic fuel blend may result in lower soot, other problems such as insufficient swelling of engine seals was reported to occur [10,11]. Hence, a minimum of 8.4 vol% aromatics content for synthetic jet fuel blend is specified under the ASTM D7566 standard [12]. Scripp *et al.* [13] tested two biojet fuels in a CFM56-5C4 engine, i.e. catalytic hydrothermolysis jet (CHJ) fuel and alcohol-to-jet (ATJ) fuel. The neat ATJ fuel, which contains <1% of aromatics, showed a reduction of 70% in PM emissions,

whereas the CHJ fuel showed an increase in PM due to higher aromatic content (20.9 vol%) and lower fuel hydrogen content. The morphology of the biojet fuel soot exhaust from a J-85 turbojet engine was examined at various thrust levels. The lower concentration of aromatics in biojet fuel blend resulted in a delayed particle inception at lower concentrations, thus allowing more dilution to occur in the fuel-rich soot region [14]. These engine tests have consistently shown that PM emissions are strongly correlated with the aromatics content, but detailed study of the combustion chemistry for biojet fuel is needed to elucidate the effect on soot formation without the complication of engine geometry and flow dynamics. Such information would be useful for soot model development and could serve as a validation target for fuel surrogate models.

The smoke point of a fuel, defined as the maximum flame height at which the fuel burns without smoking, is a standard specification in ASTM D7566 for measuring the sooting tendency of alternative jet fuel. In general, sooting tendency is inversely proportional to smoke point, where a low smoke point value indicates high sooting tendency and vice versa. Won *et al.* [15] reported that alternative jet fuels with low aromatic content exhibit considerably higher smoke point than conventional jet fuel, with FT-derived SPK showing the highest smoke point value of ~86 mm. The current ASTM D7566 specifies the minimum smoke point required for the final biojet/jet fuel blend is 25 mm or 18 mm with a maximum 3 vol% of naphthalenes, but no batch requirement on smoke point for synthetic jet fuel in neat form. The threshold sooting index (TSI), which is related to smoke point and molecular structure of fuel [16], is another method commonly employed to assess the sooting tendency of alternative jet fuel. Measurement of the smoke point of synthetic jet fuel derived from coal and gas blended with regular jet fuel at 50% vol. revealed that the soot concentration and TSI are strongly dependent on the aromatic content of the fuel [17]. Synthetic jet fuel with low aromatics content generally exhibits low sooting tendency compared to jet fuel. Although smoke point and TSI are useful indicators for assessing the sooting tendency in a practical combustor, information regarding the soot formation pathway and chemical oxidation is lacking. To examine the soot formation process at a fundamental level, a more advanced optical-based diagnostic method is needed to yield the spatial-temporal information of soot evolution in flame.

The group of Sung *et al.* [18] investigated the soot volume fraction of biojet fuel including FT-SPK, hydroprocessed esters and fatty acids from camelina (HEFA-Camelina), and alcohol-to-jet (ATJ) fuel in a non-premixed flame configuration at atmospheric conditions using laser-induced incandescence (LII). The results showed that the soot mass fraction for the less sooty alternative jet fuel is sensitive to fuel composition, strain rate and reactant concentration. Hong *et al.* [19] quantified the total soot volume of aviation bio-paraffin blended with 10-25 vol% of propylbenzene to study the soot formation in a co-flow laminar diffusion wick-fed flame using the light extinction method. It was reported that the soot concentration for bio-paraffin is only marginally different from those of straight-chain dodecane. An accurate quantification of the total soot produced in biojet fuel is useful and can serve as validation targets for fuel and flame model development, as well as enabling the prediction of soot emissions in combustor modelling.

In the present paper, the soot volume fractions of a practical biojet fuel, a synthetic paraffinic kerosene with aromatics derived from the alcohol-to-jet pathway, blends of biojet/jet fuel and surrogates of biojet fuel (39% n-dodecane, 52% iso-octane and 11% n-propylbenzene by volume) are quantified using the extinction-calibrated LII in an undiluted, pre-vaporised co-flow diffusion flame setup [20]. The technique has been shown to be a reliable method for soot quantification from a series of biofuels tests [21,22]. The spatial soot volume fraction (SVF) distribution within the flame structure of biojet flame is mapped and compared with the baseline jet fuel, followed by an investigation of the soot morphology using an electron microscope.

A numerical model is developed to simulate the 2D SVF distribution maps in the tested flames and compared with the measured data. A semi-detailed chemical kinetic mechanism for the pyrolysis and combustion of a large variety of practical fuels is employed for the calculation of gaseous phase reactions. The particle inception and size growth are modelled using a population balance method with integrated in-house reactive flow solver for multicomponent ideal gases. The model captured the key features of the SVF distribution, including distribution pattern and maximum SVF (with <10% error) in tested flames.

The present work of examining the complex fuel chemistry and formation of soot of biojet fuel at a fundamental flame level can contribute to the understanding of PM formation at engine

level.

2. Experiment

2.1 Fuel and surrogates

The biojet fuel tested in the present study is the Alcohol-to-Jet-Synthetic Kerosene with Aromatics (ATJ-SKA) produced by Swedish Biofuels AB. Selected chemical and physical properties are shown in Table 1. The fuel is composed mostly of iso- and n-alkanes, with low values of cyclo-paraffinic hydrocarbons and polyaromatics. The aromatic species in the fuel are mostly mono-aromatic. The di-aromatic content is almost negligible.

Table 1. Properties of the tested ATJ-SKA. The data in the table were provided by Swedish Biofuels AB.

Test	Method	Unit	Value
Mono-aromatic content	ASTM D 6379	wt%	11.5
Di-aromatic Content	ASTM D 6379	wt%	0.2
Poly-aromatic Content	EN 12916	wt%	<0.1
Olefins	ASTM D 1319	vol%	1.5
Density @ 15 ºC	ASTM D 4052	kg/m^3	784
Distillation IBP	ASTM D 86	˚C	160.4
Distillation FBP	ASTM D 86	˚C	260.4
Residue	ASTM D 86	vol%	1.5
Loss	ASTM D 86	vol%	0.2
Flash point	IP 170	˚C	46.0
Smoke point	ASTM D 1322	mm	27.2
Total oxygen	EN 13132	wt%	<0.2
Specific energy	ASTM D 3338	MJ/kg	43.56
Viscosity at -20 ºC	ASTM D 445	mm^2/s	3.891

The surrogates of the Jet A-1 and biojet for the modelling are listed in Table 2. The surrogate for Jet A-1 is based on three criteria: (1) atomic composition and H/C ratio; (2) degree of unsaturation (DoU); (3) fraction of cyclic alkane and aromatics. The DoU of a hydrocarbon C_nH_m is defined as $u=1+n-m/2$ [23]. The surrogate for the biojet is referred from Richter *et al.*'s previous study on the fuel [24], which follows the detailed chemical analysis depicting a typical component of the specific chemical family [25].

Table 2. Upper rows: Composition surrogate of Jet A-1; Bottom rows: biojet (Swedish Biofuels AtJ-SKA) selected for soot formation simulation. The values of the Yield Soot Indices (YSI) quoted were extracted from Ref. [23].

Jet A-1 surrogate					
Formula	**Name**	**wt%**	**Mol%**	**CAS**	**YSI**
$nC_{16}H_{34}$	n-hexadecane	50.25	37	544-76-3	11.7
$C_{10}H_{18}$	decahydronaphthalene	44.78	54	91-17-8	53.7
C_7H_8	toluene	4.97	9	108-88-3	172.5
Biojet surrogate					
$nC_{12}H_{26}$	n-dodecane	38.81	30	112-40-3	9.8
iC_8H_{18}	iso-octane	52.06	60	540-84-1	23.8
nC_9H_{12}	n-propyl benzene	9.13	10	95-63-6	260.6

The density of the two fuels are measured in the present study and shown in Table 3 along with other relevant parameters. The density of Jet A-1 (0.793 g/cm^3) and biojet (0.784 g/cm^3) are very similar, so that the volumetric blending ratio also corresponds to the mass blending ratio. The heating values of the components in the biojet surrogate are obtained from the National Institute of Standards and Technology (NIST) database [26–28], and the overall heat value of the surrogate is estimated as a weighted mean value of each component as:

$$Q = \sum_{i=1}^{n} Y_i Q_i \tag{1}$$

where Y_i and Q_i are mass fraction and heating value of each component. The calculated heating value of the biojet surrogate is 47.02 MJ/kg. The DoU of the Jet A-1 (0.95) and ATJ-SKA biojet (0.90) are also close. The DoU, u, of the surrogate is 0.40, and is estimated using Eq. (2)

$$u = \sum_{i=1}^{n} X_i u_i \tag{2}$$

where X_i and u_i are mole fraction and degree of unsaturation of each of the N components. The mean atomic composition, H/C ratio and DoU of the ATJ-SKA biojet are all remarkably similar to that of Jet A-1 (within 5% difference for each variable), while the biojet surrogate (shown in Table 2) has lower density and significantly smaller DoU.

Table 3. Properties of tested Jet A-1, biojet, and biojet surrogate. The densities were measured in

the present study using ASTM D 4052. Data of the Jet A-1 fuel are obtained from Refs. [29,30]; the formula and heating value of biojet were measured according to ASTM D3338. Heating values of the components in the biojet surrogate were obtained from the NIST database [26–28].

	Jet A-1	Biojet (B100)	Biojet surrogate (S100)
Density at 20 °C (g/cm^3)	0.793	0.784	0.723
Heat value (MJ/kg)	43.29	43.59	47.02
Average formula (-)	$C_{11}H_{22.1}$	$C_{10.5}H_{21.2}$	$C_{9.3}H_{19.8}$
H/C ratio (-)	2.009	2.019	2.130
Degree of unsaturation (-)	0.95	0.90	0.40
Stoichiometric mixture fraction Z_{st} (-)	0.0636	0.0635	0.0629
Stoichiometric flame temperature (K)	2593	2604	2754

The properties of the blended mixtures are shown in Table 4. Each mixed fuel is denoted by the volumetric blending ratio BXX, or SXX where XX is the percentage of biofuel (B) or biojet surrogate (S) in each mixture.

Table 4. Properties of the tested blending cases. Each fuel is denoted by the volumetric blending ratio BXX, or SXX where XX is the percentage of biofuel (B) or biojet surrogate (S) in each mixture.

	B10	B20	B50	B80	S10	S20	S50	S80
Density at 20 °C (g/cm^3)	0.792	0.791	0.789	0.786	0.786	0.779	0.758	0.737
Heat value (MJ/kg)	43.32	43.35	43.44	43.53	43.63	43.98	45.07	46.22
Average formula (-)	$C_{10.9}H_{22.0}$	$C_{10.9}H_{21.9}$	$C_{10.7}H_{21.6}$	$C_{10.6}H_{21.4}$	$C_{10.8}H_{21.9}$	$C_{10.6}H_{21.6}$	$C_{10.1}H_{20.9}$	$C_{9.6}H_{20.2}$
H/C ratio (-)	2.018	2.009	2.019	2.019	2.028	2.038	2.069	2.104
DoU (-)	0.94	0.94	0.92	0.91	0.89	0.83	0.67	0.50
Z_{st} (-)	0.0636	0.0636	0.0639	0.0635	0.0636	0.0635	0.0633	0.0631
Flame T (K)	2594	2595	2598	2602	2608	2623	2670	2720

2.2 Pre-vaporised diffusion flame setup

Undiluted pre-vaporised biojet fuel laminar diffusion flames are used in the present study. Soot formation in a non-premixed laminar jet flame has been extensively studied [31] and had provided a standard experiment platform for sooting propensity studies of hydrocarbon fuels. However, in most of the previous studies, the tested fuel was diluted with N_2 [32–34], argon [35], or mixed with methane [36] to lower the heat release and minimise the onset of gravity-led instability of the flame. Yet the dilution effect itself may significantly affect the soot

formation and yield in these types of flames [37]. In this study, the stability issue is resolved by using larger vapour delivery tubing and a precisely controlled evaporating system, so that dilution carrier gas is not necessary, which simplifies the analysis. The burner and fuel delivery system are shown in Fig. 1. The liquid was injected into the stainless-steel fuel tube by a precisely controlled syringe pump (Infusion ONE Syringe Pump with ± 0.5 % accuracy). A precisely controlled, closed loop, preheating system was used to heat the tube well above the boiling point of the fuels, that is, around 400°C, to make sure the fuels were fully vaporised before entering the flame. The burner is a standard non-premixed burner as used in our previous studies [31,38]. A co-flow of air at 0.18 m/s is added to protect the flame from oscillation. The operating conditions of the burner are listed in Table 5. The feeding mass rates for all cases are kept at 0.10 g/min, unless explicitly indicated.

The flame temperature for each case is estimated using the assumption of complete burning at stoichiometric conditions:

$$T_f = Y_{fu,0} Z_{st} \frac{Q}{c_p} - (T_{ox,0} - T_{fu,0}) Z_{st} + T_{fu,0} \tag{3}$$

where $Y_{fu,0}$ is the mass fraction of fuel in the fuel stream, Q the heating value from Table 3, and c_p is the specific heat of the mixture, and the value is 1.216 kJ/kg·K, which is taken as the specific heat at constant pressure (1 atm) of air at 1500 K [39]The stoichiometric mixture fraction is calculated using Eq. (4):

$$Z_{st} = \frac{Y_{ox,0} / S}{Y_{fu,0} + Y_{ox,0} / S} \tag{4}$$

where $Y_{ox,0}$ is the mass fraction of oxygen in the oxidizer stream, S is the oxygen to fuel ratio by mass at stoichiometry, which are obtained via the chemical stoichiometric calculation based on the average formula (listed in Table 4). Estimated temperature values are shown on Table 4.

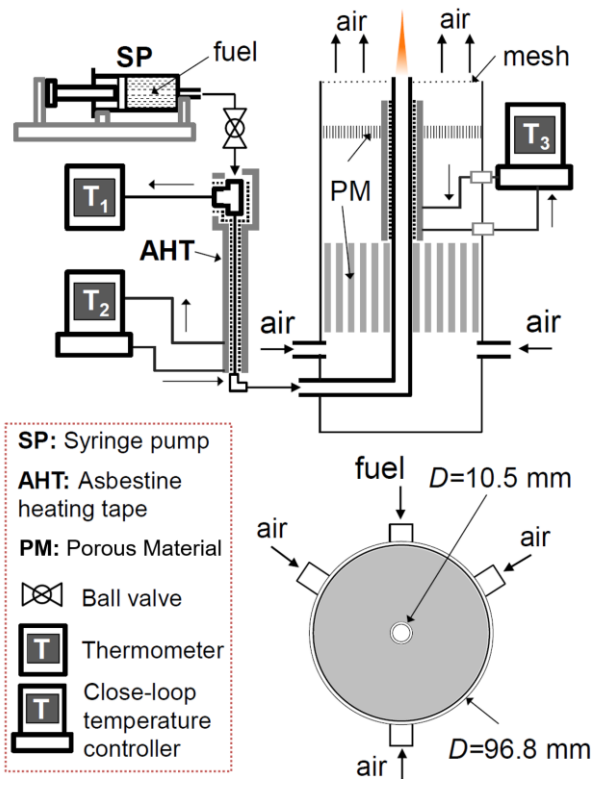

Fig. 1. Cross section (upper) and the top view (bottom) of the co-flow pre-vaporised diffusion jet flame burner.

Table 5. Geometry and operating conditions of the burner systems

Jet diameter (mm)	10
Fuel vaporisation	Fuel injection, preheat and revalorised
Fuel preheating temperature (°C)	350-390
Co-flow medium	Air
Co-flow velocity (cm/s)	18
Fuel flow rate (g/min)	0.100

2.3 Extinction calibrated planar LII system

The extinction calibrated planar 2D LII system has been proven as a robust and non-intrusive method to quantitatively measure the soot volume fraction in flames. The set-up is shown in Fig. 2, which is similar to the system used in our previous studies [37,40,41]. The laser source is a 532 nm Nd:YAG laser (Litron nanoPIV) with pulse frequency within 10–25 Hz. The laser beam was carefully expanded and trimmed into a parallel top-hat laser sheet by a series of sheet forming and trimming optics (Thorlabs cylindrical lens with focal lengths of 75, − 25 and 100 mm, respectively, and an aperture). The cross section of the laser sheet is a rectangle of

approximate dimensions, 31 mm × 0.5 mm. The top-hat laser beam energy profile was monitored using a cuvette filled with Rhodamine 6G dye, dissolved in ethanol solution. A small portion, 1% in energy terms, of the laser sheet is reflected into the cuvette to induce fluorescence and the luminosity is captured using an CCD camera (LaVision Imager Pro X 4M, 1 μs gate width, 1024 × 1024 pixels) equipped with a Nikon AF Micro Nikkor 60 mm lens (f/5.6) and a narrow band filter (Thorlabs FB600 - 10, central wavelength = 600 ± 2 nm, FWHM = 10 ± 2 nm). As the intensity of the fluorescence is proportional to the local laser energy, the shape of the fluorescence profile can be used to detect the uniformity of the energy distribution in the top-hat laser sheet.

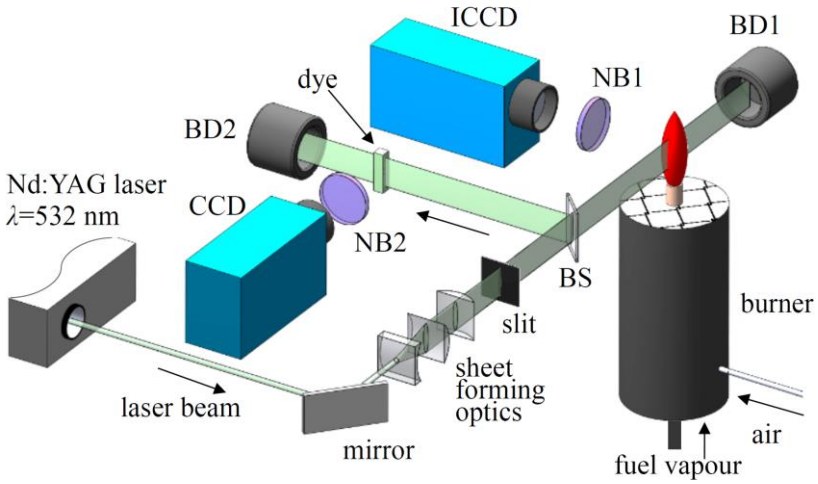

Fig. 2. Schematic of LII measurement setup. CCD Charge-Coupled Device Camera, BS beam splitter, NB1 400 ± 20 nm band filter, NB2 600 ± 5 nm band filter, BD beam dump.

The fluorescence profile in the cuvette is shown in Fig. 3(a). The representative averaged laser intensity profile over a continuous sequence of 500 shots is normalised (to 100%) as shown in the centre figure, along with the local intensity fluctuation of the laser sheet, which remains below 10%.

The dependence of the LII signal on the energy intensity per unit area (fluence) of the laser sheet was also examined. The three unblended neat cases, real Jet A-1, ATJ-SKA biojet and biojet surrogate, are tested. The mean LII intensity from HAB = 0 to 31 mm over 100 shots of the three neat fuel flames are plotted against the mean laser energy fluence of the laser sheet in Fig. 3(c). The LII signal rises with the laser fluence and reaches a plateau around 0.15 J/cm^2.

The peak level is selected to conduct the measurements, as at this point the LII signal is less sensitive to the local laser energy fluctuations.

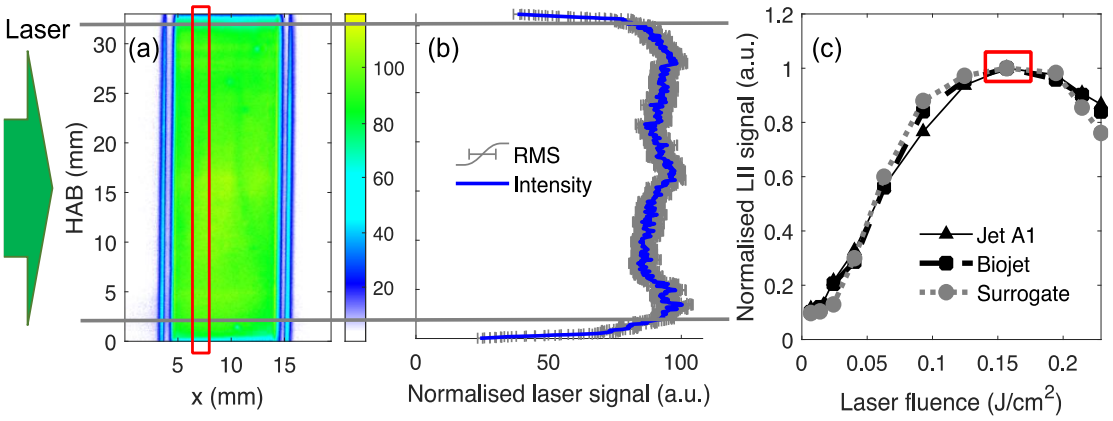

Fig. 3. (a) Rhodamine 6G fluorescence excited by laser sheet in a cuvette and (b) the normalized laser intensity profile over the vertical region along vertical coordinate HAB, as highlighted in the cuvette. The fluctuation of the laser intensity or spatial fluency is reflected in the error bars, for values below 8% of the average; (c) Fluence dependence of the LII signal for the neat Jet A-1, biojet and biojet surrogate as a function of the fluence of laser sheet. The values of LII signal intensities are normalised by the maximum value of each flame type. The peak level, highlighted by the red rectangle, is selected for the LII measurement.

The LII images were quantitatively calibrated by the line-of-sight extinction method using a 638 nm wavelength continuous-wavelength diode laser source, with correction for signal-trapping. The full details of the quantitative calibration and correction procedure can be found in previous studies [20,40].

2.4 SEM/TEM analysis

The soot produced from the flames was collected by using the thermophoretic deposition method described in Ref. [42]. A quartz plate was pre-cooled to 0°C and placed in the flame at a fixed HAB of 15 mm for a duration of less than 1 second. As all test flames are highly buoyancy controlled, a fixed sampling HAB ensures a constant residence time for the soot inception and growth. The soot sampled from the flames was cooled and examined using the LEO GEMINI 1530VP FEG-SEM system. The primary particle diameter was directly

measured from the SEM images, and the sizes of randomly selected 100 soot particles were fitted using a lognormal distribution [22].

3. Soot modelling and numerical framework

The model used for soot formation simulation employs a semi-detailed kinetic mechanism [43] for the pyrolysis and combustion of a large variety of practical fuels, including gasoline, jet fuels, diesel and biodiesel. Considering 249 chemical species and 8153 combined chemical reactions, this mechanism was developed based on hierarchical modularity and then validated using a number of experimental data sets on the laminar flame speeds of hydrocarbon and oxygenated fuels. The mechanism has been integrated in the CFD program BOFFIN, for the chemical reactions of the jet fuel and biojet surrogates, as well as the soot formation precursors. For example, long-chain alkanes, alkenes and aromatic hydrocarbons represent the composition of the practical fuels approximated in Table 2 (see Section 2.1). In addition, aromatic hydrocarbons, including naphthalene (A2), phenathrene (A3) and pyrene (A4), are set in the chemical kinetics to model the nucleation process in the soot formation.

The physical model integrates the population balance equation governing the soot particle size distribution with the in-house reactive flow solver for multicomponent ideal gases [44]. A feature of the simulation framework is a recently developed method for solving the population balance equation that combines accuracy in the prediction of the distribution with conservation of the soot volume fraction during the coagulation process. Besides detailed gas phase chemical kinetics, the model incorporates a complete set of PAH-based nucleation, condensation, HACA-based surface growth and oxidation kinetics as well as size-dependent coagulation and aggregation. Based on morphological considerations, the surface areas and geometrical properties of soot particles were estimated separately for primary particles and aggregates. The same empirical parameters in the soot model corresponding to the BBP chemical kinetics [45], obtained from a recent simulation of soot formation in an ethylene co-flow flame [46], were also used. The same soot model together with the chemical kinetics [43] in this study has been used to simulate soot formation in a co-flow flame with fuels of diesel and biodiesel surrogate [22]. The results showed that this soot model can effectively capture the reduction of soot formation on adding biodiesel fuels into diesel.

4. Results and discussion

4.1 Flame height and soot distribution

Figure 4 shows a typical comparison of soot volume fraction measurements with the simulation results, in this case for the B100 flame. The broken lines show profiles plotted in steps of 2.5 mm HAB from 5 mm to 25 mm. Both measured and model results indicate a similar soot inception HAB (the height where SVF exceeds 0.05 ppm for the first time), immediately above the nozzle exit of the burner (< 2 mm). The maximum soot volume fraction SVF_m appears in the reaction zone at the flame edge. The measured SVF_m in the B100 case is 8.3 ppm, while the modelled SVF_m in this particular case is 7.9 ppm, which is a good agreement in this particular case, and within the measurement uncertainty (~ 10%) [31] . However, the measured location of SVF_m is around 12 mm at a radius of 2 mm, which is located at a lower position than the modelled value. Similarly, in the flame centre, the soot inception takes place at HAB = 7 mm (where soot volume fraction exceeds 0.05 ppm for the first time along the stream line), which is also lower than modelled soot inception height by 3 mm. There are many possible reasons for the discrepancies, including the lack of a specific oxidation model for soot formed from these particular fuels, as well as inaccuracies in the diffusivity of the particles formed.

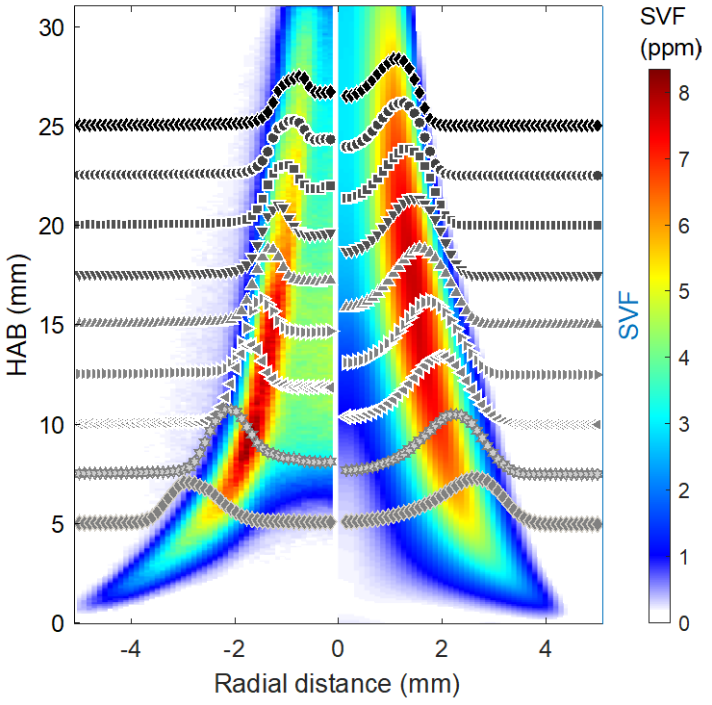

Fig. 4. Measured (left) and modelled (right) SVF in B100 flame from HAB = 0 to 31mm. Dotted lines show profiles plotted in steps of 2.5 mm HAB.

Figure 5 shows the natural luminous photos of flames and soot volume fraction (SVF) distribution in the tested Jet A-1 and biojet blending flames. The SVF data for the cases in Fig. 5 are attached in the form of a readable TIFF figure in the Appendix. Each panel of two rows shows photos of each case in the top row, and on the second row of the pair, the measured SVF on the left half of each case, and the modelled results on the right half. On the bottom two rows, the flow rate of fuel is indicated in parentheses as in g/min (05) or (15).

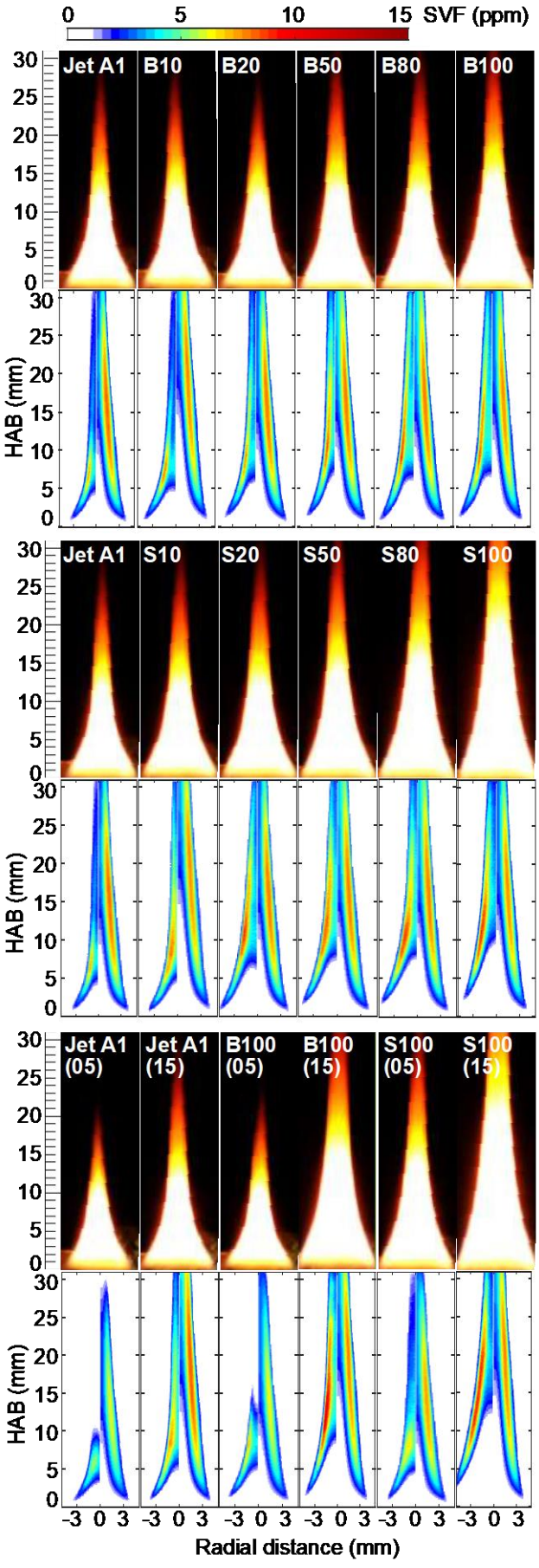
0 5 10 15 SVF (ppm)
Jet A1
B10
B20
B50
B80
B100
S10
S20
S50
S80
S100
Jet A1 (05)
Jet A1 (15)
B100 (05)
B100 (15)
S100 (05)
S100 (15)
HAB (mm)
Radial distance (mm)

299

Fig. 5. Each panel of a pair of rows shows photos of each case in the top row, followed by a bottom row containing the measured SVF on the left half of each case, and the modelled results on the right half. The fuel is denoted by the volumetric blending ratio BXX, or SXX where XX is the percentage of biofuel (B) or biojet surrogate (S) in each mixture. On the bottom two rows, the fuel flow rate is indicated in parentheses as in g/min (05) or (15).

Figure 5 shows that the visible luminous flame height of the cases in the top panel are similar. According to the diffusion theory of jet flames [47–49], when the flame is dominated by high buoyancy- and the initial flow velocity is ignored, the flame height H_f of a cylindrical diffusion jet flame can be estimated as:

$$H_f = \frac{22400\dot{m}}{4\pi D_0 MW \cdot \ln(1+S^{-1})}\left(\frac{T_0}{T_f}\right)^{0.67} \quad (5)$$

where $\dot{m}$ is the fuel mass consumption rate in kg/s; D_0 is the diffusion coefficient of the mixture in m^2/s at the reference temperature T_0; MW is the molecular weight of the fuel. Table 4 shows that the values T_f of Jet A-1 and biojet are similar; moreover, as the mean formula of Jet A-1 and biojet are similar, the MW and S of fuels are also similar. Assuming a constant value of D_0 in tested flames of Jet A-1, biojet and their blending (first row of Fig. 5), the visible flame heights should be very similar. The measured H_f of the flames in the first row is within the range 28±3 mm, which is about twice the predicted H_f using Eq. 5 (~13 mm). The large discrepancy between the calculated and measured H_f could be caused by an insufficient soot oxidation reaction time, and the absence of heat loss via radiation in the model, which results in overestimations of the flame temperature, the reaction rate and hence the required residence time is shorter and a smaller H_f is predicted [50].

A comparison across the measured SVF maps of Jet A-1, B10 to B100 cases (left panel in each subfigure of the second row of Fig. 5) shows the SVF distribution patterns are very similar in these cases. Along the flame edge, soot appears very close to the burner nozzle (HAB < 2 mm) and grows along the streamline until it reaches a maximum soot volume fraction (SVF_m). At the flame centre, the soot formation is delayed due to heat transfer from the flame edge to the centre [51], thus the HAB where soot appears is higher than that at flame edge by 4-7 mm. In

all tested biojet/Jet A-1 flames (first row), the soot model roughly captures the typical distribution pattern of soot in the co-flow diffusion hydrocarbon jet flame: the maximum SVF appears along the streamline at the flame edge (the annular region of the cylindrical flame), rather than along the flame centreline. However, there are key discrepancies between the experimental and modelling data: (1) along the flame centre, the measured sooting points (the HAB where SVF exceeds 0.05 ppm for first time) are lower than the predicted ones; (2) at the annular region, the distribution of the soot is slightly broader than the measured patterns. As discussed in the context of Fig. 4, discrepancies may be caused by the inaccuracies in chemical model and species diffusivities. The current model includes many reactions, including light hydrocarbons, PAHs, several long-chain alkanes, alkenes and saturated and non-saturated methyl esters. Yet model validation relies on results for sooting from gaseous flames. The model requires as input fuel composition, ratio of carbon-hydrogen-oxygen, bond saturation and heating values. Soot modelling relies on empirical parameters calibrated accorsing to the measured soot morphology (average primary particle size) in ethylene flames [44], rather than the present biojet or Jet A-1 fuel flames. Therefore, rates of formation of key species including C_2H_2, OH, PAHs may not be accurate, thus directly affecting the predictions of the soot model.

Luminosity and SVF for flames of neat biojet surrogate (S100) and their blends with Jet A-1 (S10, S20, S50, S80) are shown in the middle rows of Fig. 5, showing a slight increase in H_f with blending ratio, as well as higher SVF values distributed over a higher distance. This is consistent with higher soot propensity in the biojet surrogate/Jet A-1 flame compared to pure Jet A-1. The estimated diffusion flame temperature of the biojet surrogate is the highest (~2754 K) comparing the Jet A-1 (~2593 K) and biojet flames (~2604 K), which could lead to higher rates of soot formation, and thus visible luminosity. A direct measurement of the temperature in the tested heavy sooting flames was difficult as the soot particles easily deposit on the tip of the thermocouple. The comparison between the model and experimental results of the biojet surrogate + Jet A-1 flames (S10, S20, S50, S80, S100 cases, the second line in Fig. 5) shows similar disagreements with the measured values, as discussed above.

The third pair of rows in Fig. 5 shows the neat Jet A-1, biojet and surrogate flames for reduced and increased fuel flow rates of 0.05 g/min (jet A1 (05), B100(05), S100(05)) and 0.15 g/min

(jet A1(15), B100(15), S100(15)), respectively. Given the expected proportionality suggested in Eq. (5), it is not surprising that the luminous flame height of Jet A-1 (05) is lower than Jet A-1 (fuel consumption rate is 0.10 g/min) flame by 10 mm (70%). The measured SVF in Jet A-1 (05) is also lower than Jet A-1(10) flame, as the residence time for soot particle growth is limited. The reduction of SVF in the Jet A-1 (05) flame compared to the Jet A-1 flame is captured by the model, but model predictions of the flame height are about twice the measured value. The Jet A-1(15) flame has neither a higher flame nor significantly larger SVF than Jet A-1(10) flame. This might be because the radiation loss in the heavy sooting flames is significant. When fuel consumption rate increases from 0.10 g/min to 0.15 g/min, the soot yielding increases and the heat loss via soot radiation become a dominant factor reducing the flame temperature and the flames were quenched. Some unburnt fuel vapour was emitted from the flame tip together with soot particles. The same trend was also observed in the B100(15) and S100(15) cases. A parallel comparison among the measured SVF maps of neat Jet A-1, biojet and biojet surrogate cases shows that high SVF region at flame edge extend further downstream for the B100 and S100 flames compared with the Jet A-1 flame. This trend is even more pronounced for Jet A1 (15) compared with B100 (15) and S100 (15). This might be caused by a higher radiation loss in the B100 (15) and S100 (15) flames. The loss resulted in a lower flame temperature in the downstream of B100 (15) and S100 (15) flames and the oxidation of soot in are hence delayed. In general, as shown in Fig. 5, blending of biojet with the Jet A-1 does not fundamentally change the flame structure and soot distribution in the tested diffusion flames. The surrogate could reasonably represent the sooting propensity of the biojet fuel. As shown in Figs. 4 and 5, the model reasonably and quantitatively captures the distribution of SVF_m soot within the tested flames. However, differences in chemical composition and oxidation rates may not be perfectly captured, and similarly the absence of details on radiation losses may overestimate the temperatures, leading to differences in both soot formation and oxidation.

4.3 Maximum and mean soot volume fraction

The maximum soot volume fraction, SVF_m .in the tested cases are plotted in Fig. 6 against the volumetric blending ratio of biojet (upper) and biojet surrogate (bottom) with Jet A-1 fuel. The error bars in of the measured values are calculated based on the standard deviations of 20 LII

images for each case. The SVF_m in the biojet blending cases varies from 7.8 ppm (B20) to 8.4 ppm (B80). Considering the uncertainty of the LII measurement of approximately 10%, the difference between the two values is insignificant. Thus, it is reasonable to conclude that the addition of the ATJ-SKA biojet does not change the soot yield of Jet A-1 fuel in terms of the maximum soot volume fraction. It is worthy to pointed out is that these SVF values shown in Figs 4, 5 and 6 also contains calibration uncertainties besides the random measurement uncertainty. Due to the nature of the optical measurement of soot, the calibration uncertainties could be as high as 40% [31]. The calibration process and uncertainty were analysed in detail in our previous study [31]. The interaction between light beam and soot particles is highly complex, as it depends on the wavelength of probing beam, maturity and chemical composition of soot (e.g. H/C ratio) [52], thus the calibration uncertainty is difficult to be quantified and hence was not shown in Fig. 6. However, the calibration affects the SVF measurement in a linear manner, thus it does not change the conclusion drawn in the present study, which are based on the relative comparison among the teste fuels.

The modelled SVF_m agrees with the measured data within the range of measurement uncertainty in all tested cases, which is impressive. The bottom part of Fig. 6 shows that the blended cases of biojet surrogate with the Jet A-1 produce higher SVF_m than the biojet/Jet A-1 blending cases by a small margin (<15%) in all corresponding cases. Our previous studies on petroleum and bio diesels show that the degree of unsaturation (DoU) of the fuels may play a key role in the sooting propensities of fuels [40].

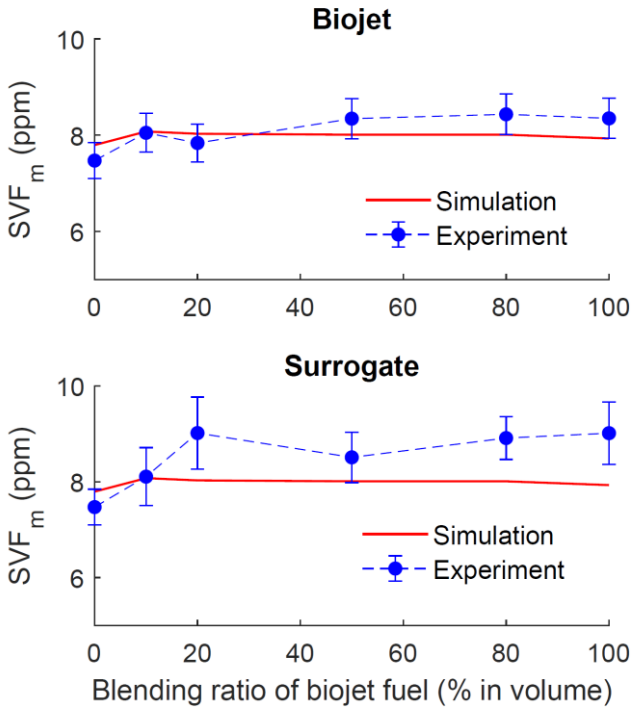

405

406 **Fig. 6.** Maximum soot volume fraction against the blending ratio of biojet fuel (upper) and

407 surrogate (bottom)

408 The DoU of the Jet A-1 and biojet shown in Table 3 (Section 2.1) 0.95 and 0.90, respectively,
409 whereas the DoU of the biojet surrogate is 0.40. So, it is very surprising to observe higher soot
410 values than the Jet A-1 and ATJ-SKA biojet, which is the opposite of the expected effect.

411 The Yield Soot Indices (YSI) is another indicator of the sooting propensity of jet fuels
412 [23,36,53]. The YSI of the surrogates for the Jet A-1 and biojet fuels are estimated as a mean
413 of the molar weighted values:

414 $$\mathrm{YSI} = \sum_{i=1}^{n} X_i \mathrm{YSI}_i \qquad (6)$$

415 The YSI of each component of the surrogate for the Jet A-1 and biojet are obtained from [23]
416 (listed in the Table 2). Based on the YSI values in Table 2, the calculated YSI values for the
417 surrogate of biojet and Jet A-1 are 43.27 and 48.84 respectively. The YSI of the biojet surrogate
418 is lower than the Jet A-1 surrogate by 11%, whereas the biojet surrogate produces 15% higher
419 SVF_m than biojet and Jet A-1. The modelled values of SVF_m in the neat jet A1 case (7.8 ppm)
420 is slightly lower than that in the neat biojet surrogate case (7.9 ppm) and indicates a comparison
421 opposite to that indicated by the YSI. One possible explanation for the higher soot yield of the

surrogate than Jet A-1 may be the presence of aromatic species. Previous studies show that the soot yielding of jet fuels are very sensitive to the presence of aromatic species in the fuels [30,54]. In the present study, the surrogate for the Jet A-1 contains 4.97% toluene C_7H_8 in mass, which is less than the propylbenzene (C_9H_{12}) mass fraction of 9.13% in the biojet surrogate, so it is reasonable that the Jet A-1 surrogate produce less soot than biojet surrogate. However, the YSI of decahydronaphthalene (53.7) is significantly higher than iso-octane (23.8), the calculated overall YSI of Jet A-1 (contains 44.78% decahydronaphthalene in mass) is hence slightly higher than biojet surrogate (contains 52.06% iso-octane in mass). Obviously, due to the high fraction of aromatics, the biojet surrogate overestimated the sooting tendency of the tested ATJ-SKA, but due to the presence of iso-octane (with very low YSI), the overestimation was not reflected by the value of YSI. The present study suggested that the fraction of aromatics, rather than YSI, may be a better indicator of a fuel's sooting characteristics.

A second measure of soot propensity may be given by the radially averaged soot volume fractions SVF_a, which is evaluated from the 2D soot distribution via Eq. (7).

$$SVF_a = \frac{1}{\pi R^2}\int_0^R 2\pi r SVF(r)\, dr \tag{7}$$

The calculated results for SVF_a are plotted against HABs in Fig. 7. The biojet surrogate/Jet A-1 mixtures yield larger SVF_a than the biojet/Jet A-1 mixtures except the B10 case. However, at higher HABs (>20 mm), the values become closer. Around 31 mm, the SVF_a values for biojet surrogate/Jet A-1 mixtures and biojet/Jet A-1 mixtures are almost equal. The model predicts more soot in B0 to B50 cases, while in B80 and B100 cases, the peak SVF_a predicted by the model is lower than the biojet surrogate/Jet A-1 mixtures but higher than the biojet/Jet A-1 mixtures.

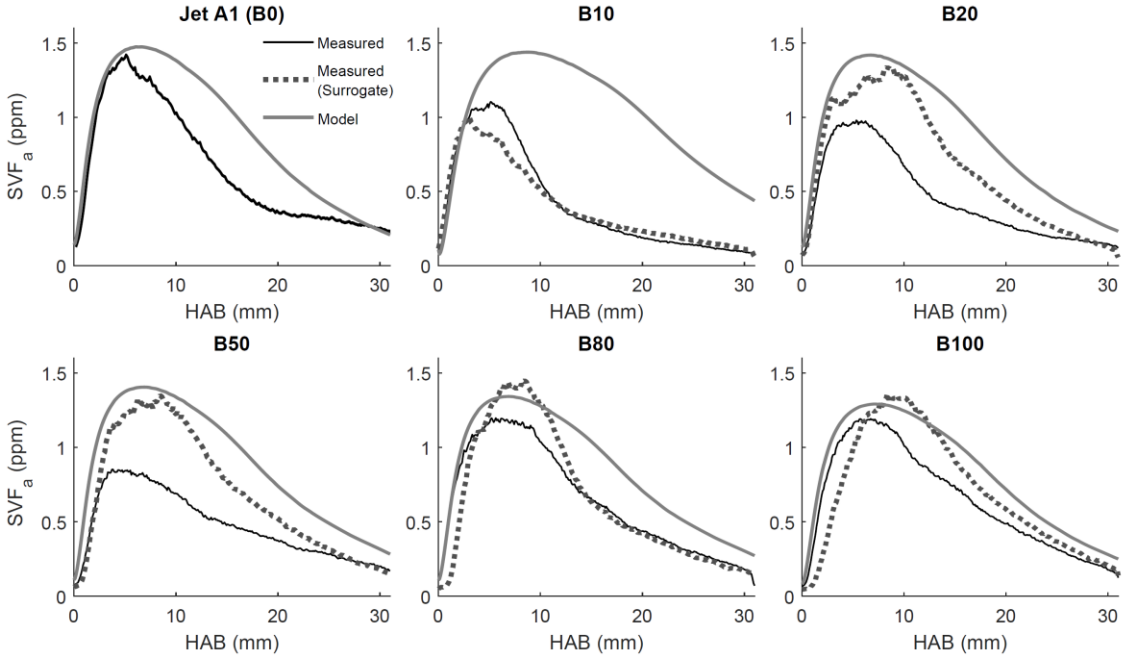

Fig. 7. Averaged SVF_a along HABs in tested cases

4.4 Primary soot particle size and number density

SEM images and corresponding particle size distributions for tested Jet A-1, biojet and biojet surrogate pre-vaporised diffusion flames are shown in Fig. 8.

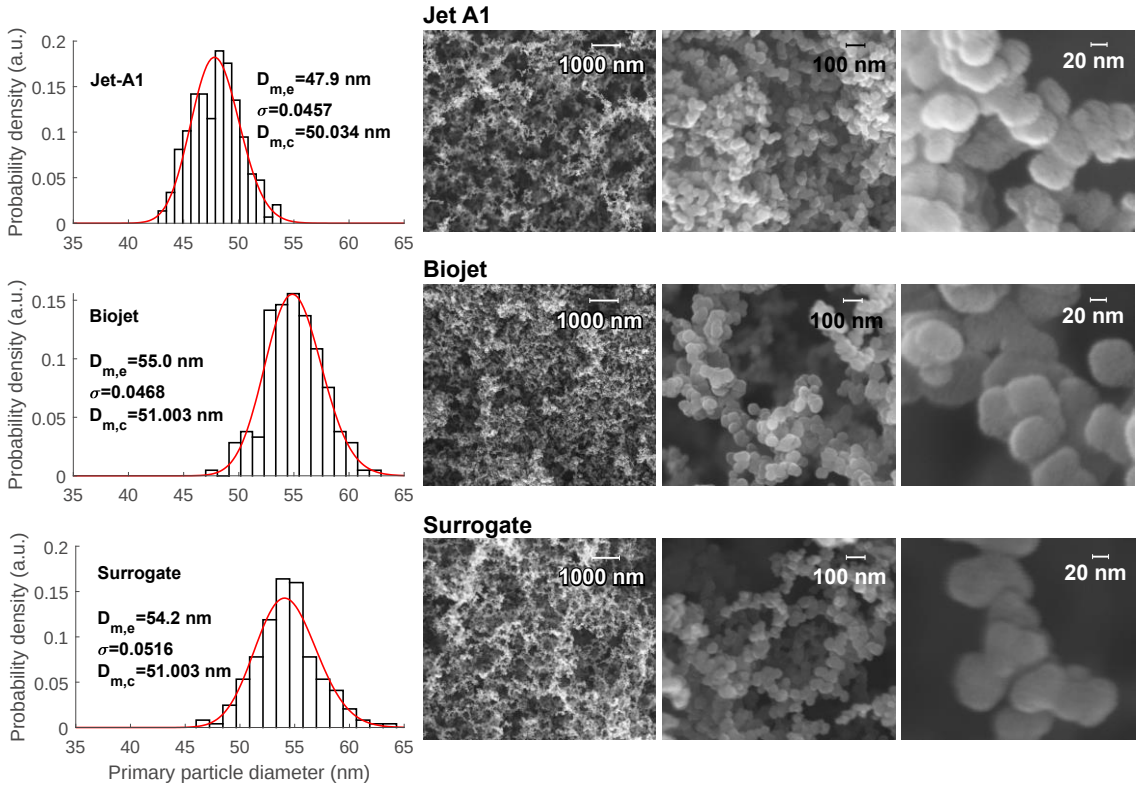

Fig. 8. SEM images and corresponding particle size distribution for tested Jet A-1, biojet (Swedish Biofuels ATJ) and biojet surrogate pre-vaporised diffusion flames.

The soot number density is estimated from the averaged soot volume fraction SVF_a, assuming particles of geometric mean agglomerate diameter D_m as determined from sampling and analysis of SEM images, via:

$$N_p = \frac{6 \cdot \mathrm{SVF_a}}{\pi D_m^3} \tag{8}$$

Estimates are only available at HAB = 15 mm, from which the data were sampled. The simulation results are shown in Table 6.

Table 6. Measured average soot volume fraction SVF_a, mean primary particle diameter D_m and estimated particle number density N_p at HAB = 15 mm for neat Jet A-1 (B0), Biojet (B100) and biojet surrogate (S100) cases

	SVF_a (ppm)	**D_m** (nm)	**N_p** (10^{13}·m^{-3})
Jet A-1	0.57	47.9	9.9
Biojet	0.72	55.0	8.3
Biojet surrogate	0.80	54.2	9.6

As shown in Table 6, although the SVF_a at HAB=15 mm in neat Jet A-1 flame is 20% and 28% lower than neat biojet and biojet surrogate flame, respectively, the mean values of N_p at HAB = 15 mm for Jet A-1 flame, the value of N_p in Jet A-1 flame is 19% and 3% higher than the neat biojet and biojet surrogate cases. The results indicate that tested ATJ-SKA biojet produces larger but less soot particles than the Jet A-1 fuel. The finding also implies the soot particle nucleation in the Jet A-1 flame is more frequent than the biojet and biojet surrogate, while the surface growth of soot particles is slower comparing the biojet and biojet surrogate flames. The measured primary particle size of the soot particles produced in the neat biojet flame and biojet surrogate flame are very similar and the difference in the mean diameter is within 2%. Both results agree well with the simulation data. The modelled soot particle size for distribution the neat Jet A-1, biojet and the biojet surrogate are noted as $D_{m,c}$ and shown in Fig. 8, which agree well with the measured data. The model also successfully predicted that the Jet A-1 produced smaller particles than the other two fuels, but the difference is very narrow (< 1 nm). This

indicates that the model may not be very sensitive in the prediction of the particle size produced in the different fuels, and the mechanism for soot surface growth in the model, which dominates the soot particle size, may need further adjustment.

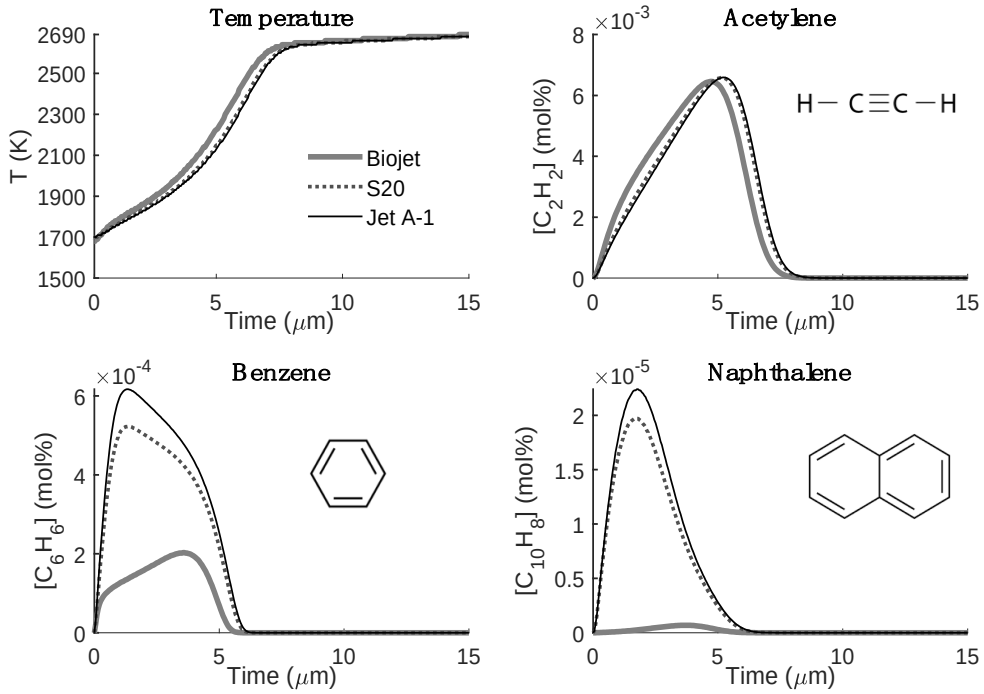

Fig. 9. Temperature, mole fractions of acetylene C_2H_2, benzene C_6H_6 and naphthalene $C_{10}H_8$ produced in the combustion of the neat ATJ-SKA biojet, S20 biojet surrogate, and neat Jet A-1 surrogate.

To investigate the combustion performance of different chemical compositions and the effect on soot formation, simulations of a perfect stirred reactor have been conducted in Reaction Design's CHEMKIN-PRO commercial software with the semi-detailed mechanism. Three fuel compositions have been studied in the stoichiometric air-fuel condition: pure jet fuel, biojet fuel and the blend fuel with 20% biojet and 80% Jet A-1 (B20). The initial temperature is set at 1700 K for an easy ignition. The results of key species regarding soot formation are monitored, including acetylene C_2H_2 and PAHs. The temperature, mole fractions of acetylene, benzene C_6H_6 and naphthalene $C_{10}H_8$ are plotted against time in the Fig. 9. The temperature of the biojet surrogate increases faster than Jet A-1 surrogate. Benzene and naphthalene are the key species for soot inception, as they provide the first ring for the nascent soot particle nucleation [55,56].

The rate of formation of benzene and naphthalene in the ATJ-SKA biojet and S20 cases are lower than in the Jet A-1 flame. Indeed, the rate of formation of naphthalene in the ATJ-SKA biojet is negligible. This may explain the fact that the number density of soot in biojet flame is smaller than Jet A-1 flame. The yield of acetylene, the main species responsible for soot particle surface growth based on HACA mechanism, is very similar in the three cases, thus, the total soot yielding of the tested flames are in a same level.

5. Conclusion

The soot volume fraction and primary particle size in the pre-vaporised diffusion flames of an ATJ-SKA biojet fuel and its blends with Jet A-1 have been studied both experimentally and numerically. The visible flame height, spatial soot volume fraction distribution, and the maximum soot volume fraction SVF_m of neat ATJ-SKA biojet fuel and its blends with Jet A-1 are close to those found for neat Jet A-1 fuel flames. The difference in SVF_m is within 8% and smaller than the measurement uncertainty. It is reasonable to conclude that the sooting propensity of the ATJ-SKA does not differ from standard Jet A-1 fuel. The flames using the biojet surrogate produce slightly more soot than the equivalent flames with biojet and Jet A-1. Both the values of SVF_m and SVF_{mean} produced in neat biojet surrogate fuel flames are higher than the values in neat biojet flames by 8.1% and 20%, respectively. Since the DoU of the biojet surrogate is lower than biojet, the results show that it is not the determinant factor for the sooting propensity of biojet fuels. This point should be taken into account in the design of jet fuel surrogates. The neat Jet A-1 produces finer soot particles and larger number density than ATJ-SKA biojet and the biojet surrogate. The result indicates the soot particle inception in the Jet A-1 flame is more frequent than the biojet and biojet surrogate, while the surface growth of soot particles is slower than the biojet and biojet surrogate flames. A simulation of the production of flame soot provides support for this conclusion. The soot model successfully predicted the soot distribution and SVF_m in the tested neat biojet case and the blended cases with Jet A-1 fuels. The differences between the measured and modelled SVF_m are within 10% of each other in all cases. In addition, the predicted soot primary particle size is within 10% of the measured values. However, the predicted SVF_a is significantly higher than the experimental data, showing the

519 model still needs further development.

520 Acknowledgement

521 C. T. Chong is supported by the Newton Advanced Fellowship of the Royal Society
522 (NA160115). Anxiong Liu gratefully acknowledges the financial support of the Chinese
523 Scholarship Council (CSC) and the EPSRC grant No. EP/S012559/1.

524 List of supplementary material

525 Soot Volume Fraction.tif

526 References

527 [1] Stratton RW, Wong HM, Hileman JI. Life cycle green house gas emissions from
528 alternative jet fuels. Partnership of Air Transportation Noise and Emissions Reduction.
529 Cambridge, MA: Massachusetts Institute of Technology 2010.
530 http://web.mit.edu/aeroastro/partner/reports/proj28/partner-proj28-2010-001.pdf.
531 [2] Ganguly I, Pierobon F, Bowers TC, Huisenga M, Johnston G, Eastin IL. 'Woods-to-
532 Wake' Life Cycle Assessment of residual woody biomass based jet-fuel using mild
533 bisulfite pretreatment. Biomass and Bioenergy 2018;108:207–16.
534 https://doi.org/10.1016/j.biombioe.2017.10.041.
535 [3] Fan J, Shonnard DR, Kalnes TN, Johnsen PB, Rao S. A life cycle assessment of
536 pennycress (Thlaspi arvense L.) -derived jet fuel and diesel. Biomass and Bioenergy
537 2013;55:87–100. https://doi.org/10.1016/j.biombioe.2012.12.040.
538 [4] Wei C-F, Larson SM, Patten KO, Wuebbles DJ. Modeling of ozone reactions on
539 aircraft-related soot in the upper troposphere and lower stratosphere. Atmos Environ
540 2001;35:6167–80. https://doi.org/10.1016/S1352-2310(01)00409-5.
541 [5] Xu H, Fu Q, Yu Y, Liu Q, Pan J, Cheng J, et al. Quantifying aircraft emissions of
542 Shanghai Pudong International Airport with aircraft ground operational data. Environ
543 Pollut 2020;261:114115. https://doi.org/10.1016/j.envpol.2020.114115.
544 [6] EU. European Union Aviation Safety Agency, European Aviation Environmental
545 Report. 2019.

[7] Han B, Goh H, Tung C, Ge Y, Chyuan H, Ng J, et al. Progress in utilisation of waste cooking oil for sustainable biodiesel and biojet fuel production. Energy Convers Manag 2020;223:113296. https://doi.org/10.1016/j.enconman.2020.113296.

[8] Huang CH, Vander Wal RL. Effect of soot structure evolution from commercial jet engine burning petroleum based JP-8 and synthetic HRJ and FT fuels. Energy and Fuels 2013;27:4946–58. https://doi.org/10.1021/ef400576c.

[9] Lobo P, Hagen DE, Whitefield PD. Comparison of PM emissions from a commercial jet engine burning conventional, biomass, and fischer-tropsch fuels. Environ Sci Technol 2011;45:10744–9. https://doi.org/10.1021/es201902e.

[10] Link DD, Gormley RJ, Baltrus JP, Anderson RR, Zandhuis PH. Potential additives to promote seal swell in synthetic fuels and their effect on thermal stability. Energy and Fuels 2008;22:1115–20. https://doi.org/10.1021/ef700569k.

[11] Jürgens S, Oßwald P, Selinsek M, Piermartini P, Schwab J, Pfeifer P, et al. Assessment of combustion properties of non-hydroprocessed Fischer-Tropsch fuels for aviation. Fuel Process Technol 2019;193:232–43. https://doi.org/10.1016/j.fuproc.2019.05.015.

[12] ASTM. International, D7566-19b, Standard specification for aviation turbine fuel containing synthesized hydrocarbons, 2019,. 2019.

[13] Schripp T, Herrmann F, Oßwald P, Köhler M, Zschocke A, Weigelt D, et al. Particle emissions of two unblended alternative jet fuels in a full scale jet engine. Fuel 2019;256:115903. https://doi.org/10.1016/j.fuel.2019.115903.

[14] Kumal RR, Liu J, Gharpure A, Vander Wal RL, Kinsey JS, Giannelli B, et al. Impact of Biofuel Blends on Black Carbon Emissions from a Gas Turbine Engine. Energy and Fuels 2020;34:4958–66. https://doi.org/10.1021/acs.energyfuels.0c00094.

[15] Won SH, Veloo PS, Dooley S, Santner J, Haas FM, Ju Y, et al. Predicting the global combustion behaviors of petroleum-derived and alternative jet fuels by simple fuel property measurements. Fuel 2016;168:34–46. https://doi.org/10.1016/j.fuel.2015.11.026.

[16] Calcote HF, Manos DM. Effect of molecular structure on incipient soot formation.

575 Combust Flame 1983;49:289–304. https://doi.org/10.1016/0010-2180(83)90172-4.
576 [17] Han HS, Kim CJ, Cho CH, Sohn CH, Han J. Ignition delay time and sooting
577 propensity of a kerosene aviation jet fuel and its derivative blended with a bio-jet fuel.
578 Fuel 2018;232:724–8. https://doi.org/10.1016/j.fuel.2018.06.032.
579 [18] Xue X, Hui X, Singh P, Sung CJ. Soot formation in non-premixed counterflow flames
580 of conventional and alternative jet fuels. Fuel 2017;210:343–51.
581 https://doi.org/10.1016/j.fuel.2017.08.079.
582 [19] Hong TD, Fujita O, Soerawidjaja TH, Reksowardojo IK. Soot formation of dodecane,
583 aviation bio-paraffins and their blends with propylbenzene in diffusion flames. Renew
584 Energy 2019;136:84–90. https://doi.org/10.1016/j.renene.2018.12.105.
585 [20] Chong CT, Tian B, Ng JH, Fan L, Ni S, Wong KY, et al. Quantification of carbon
586 particulates produced under open liquid pool and prevaporised flame conditions:
587 Waste cooking oil biodiesel and diesel blends. Fuel 2020;270:117469.
588 https://doi.org/10.1016/j.fuel.2020.117469.
589 [21] Tian B, Chong CT, Fan L, Ng J-H, Zhang C, Hochgreb S. Soot volume fraction
590 measurements over laminar pool flames of biofuels, diesel and blends. Proc Combust
591 Inst 2019;37:877–84. https://doi.org/10.1016/j.proci.2018.05.094.
592 [22] Tian B, Liu AX, Chong CT, Fan L, Ni S, Ng J-H, et al. Experimental and numerical
593 study on soot formation inlaminar diffusion flames of biodiesels and methyl esters.
594 Proceeding Combust Inst 2020.
595 [23] Das DD, McEnally CS, Kwan TA, Zimmerman JB, Cannella WJ, Mueller CJ, et al.
596 Sooting tendencies of diesel fuels, jet fuels, and their surrogates in diffusion flames.
597 Fuel 2017;197:445–58. https://doi.org/10.1016/j.fuel.2017.01.099.
598 [24] Richter S, Naumann C, Kathrotia T, Riedel U. Synthesized Alternative Kerosenes –
599 Characterization through Experiments and Modeling. Proc. Eur. Combust. Meet.,
600 2019. https://doi.org/elib.dlr.de/128734/.
601 [25] Zschocke A, Scheuermann S. High Biofuel Blends in Aviation (HBBA). 2012.
602 [26] NIST. Benzene, propyl- (NIST Chemistry WebBook, SRD 69) n.d.
603 https://webbook.nist.gov/cgi/cbook.cgi?ID=C103651&Mask=4 (accessed June 1,

2020).

[27] NIST. Pentane, 2,2,4-trimethyl- (NIST Chemistry WebBook, SRD 69) n.d. http://webbook.nist.gov/cgi/cbook.cgi?ID=C540841&Units=CAL&Type=IR-SPEC (accessed June 1, 2020).

[28] NIST. Dodecane (NIST Chemistry WebBook, SRD 69) n.d. https://webbook.nist.gov/cgi/cbook.cgi?ID=C112403&Mask=FFF (accessed June 1, 2020).

[29] de Oliveira PM, Mastorakos E. Mechanisms of flame propagation in jet fuel sprays as revealed by OH/fuel planar laser-induced fluorescence and OH* chemiluminescence. Combust Flame 2019;206:308–21. https://doi.org/10.1016/j.combustflame.2019.05.005.

[30] Braun-Unkhoff M, Riedel U, Wahl C. About the emissions of alternative jet fuels. CEAS Aeronaut J 2017;8:167–80. https://doi.org/10.1007/s13272-016-0230-3.

[31] Tian B, Gao Y, Balusamy S, Hochgreb S. High Spatial Resolution Laser Cavity Extinction and Laser Induced Incandescence in Low Soot Producing Flames. Appl Phys B Lasers Opt 2015;120:469–87. https://doi.org/10.1007/s00340-015-6156-3.

[32] Gao Z, Zhu L, Zou X, Liu C, Tian B, Huang Z. Soot reduction effects of dibutyl ether (DBE) addition to a biodiesel surrogate in laminar coflow diffusion flames. Proc Combust Inst 2018;000:1–8. https://doi.org/10.1016/j.proci.2018.05.083.

[33] Kholghy MR, Weingarten J, Sediako AD, Barba J, Lapuerta M, Thomson MJ. Structural effects of biodiesel on soot formation in a laminar coflow diffusion flame. Proc Combust Inst 2017;36:1321–8. https://doi.org/10.1016/j.proci.2016.06.119.

[34] Matti Maricq M. Physical and chemical comparison of soot in hydrocarbon and biodiesel fuel diffusion flames: A study of model and commercial fuels. Combust Flame 2011;158:105–16. https://doi.org/10.1016/j.combustflame.2010.07.022.

[35] Abboud J, Schobing J, Legros G, Matynia A, Bonnety J, Tschamber V, et al. Impacts of ester's carbon chain length and concentration on sooting propensities and soot oxidative reactivity: Application to Diesel and Biodiesel surrogates. Fuel 2018;222:586–98. https://doi.org/10.1016/j.fuel.2018.02.103.

633 [36] Das DD, McEnally CS, Pfefferle LD. Sooting tendencies of unsaturated esters in
634 nonpremixed flames. Combust Flame 2015;162:1489–97.
635 https://doi.org/10.1016/j.combustflame.2014.11.012.
636 [37] Tian B, Gao Y, Zhang C, Hochgreb S. Soot measurement by combining continuous
637 wave multipass extinction and laser-induced incandescence in diluted methane flames.
638 Combust Flame 2018;192:224–37.
639 https://doi.org/10.1016/j.combustflame.2018.01.037.
640 [38] Tian B, Zhang C, Gao Y, Hochgreb S. Planar 2-Colour Time-Resolved Laser-Induced
641 Incandescence Measurements of Soot in a Diffusion Flame. Aerosol Sci Technol
642 2017;51:1345–53. https://doi.org/10.1080/02786826.2017.1366644.
643 [39] Urieli I. Ohio Univeristy - Specific Heat Capacities of Air n.d.
644 https://www.ohio.edu/mechanical/thermo/property_tables/air/air_Cp_Cv.html
645 (accessed June 1, 2020).
646 [40] Tian B, Chong CT, Fan L, Ng J-H, Zhang C, Hochgreb S. Soot volume fraction
647 measurements over laminar pool flames of biofuels, diesel and blends. Proc Combust
648 Inst 2018;37:877–84. https://doi.org/10.1016/j.proci.2018.05.094.
649 [41] Tian B. Laser diagnostics of soot in hydrocarbon diffusion flames. University of
650 Cambridge, 2016. https://doi.org/https://doi.org/10.17863/CAM.56369.
651 [42] Merchan-Merchan W, Abdihamzehkolaei A, Merchan-Breuer DA. Formation and
652 evolution of carbon particles in coflow diffusion air flames of vaporized biodiesel,
653 diesel and biodiesel-diesel blends. Fuel 2018;226:263–77.
654 https://doi.org/10.1016/j.fuel.2018.02.183.
655 [43] Ranzi E, Frassoldati A, Grana R, Cuoci A, Faravelli T, Kelley AP, et al. Hierarchical
656 and comparative kinetic modeling of laminar flame speeds of hydrocarbon and
657 oxygenated fuels. Prog Energy Combust Sci 2012;38:468–501.
658 https://doi.org/10.1016/j.pecs.2012.03.004.
659 [44] Liu A, Rigopoulos S. A conservative method for numerical solution of the population
660 balance equation, and application to soot formation. Combust Flame 2019;205:506–
661 21. https://doi.org/10.1016/j.combustflame.2019.04.019.

[45] Blanquart G, Pepiot-Desjardins P, Pitsch H. Chemical mechanism for high temperature combustion of engine relevant fuels with emphasis on soot precursors. Combust Flame 2009;156:588–607. https://doi.org/10.1016/j.combustflame.2008.12.007.

[46] Liu AX, Garcia CE, Sewerin F, Williams BAO, Rigopoulos S. Population balance modelling and laser diagnostic validation of soot particle evolution in laminar ethylene diffusion flames. Combust Flame n.d.:Accepted.

[47] Roper FG. The prediction of laminar jet diffusion flame sizes: Part I. Theoretical model. Combust Flame 1977;29:219–26. https://doi.org/10.1016/0010-2180(77)90112-2.

[48] Roper FG, Smith C, Cunningham a. C. The prediction of laminar jet diffusion flame sizes: Part II. Experimental verification. Combust Flame 1977;29:227–34. https://doi.org/10.1016/0010-2180(77)90113-4.

[49] Olson DB, Pickens JC, Gill RJ. The effects of molecular structure on soot formation II. Diffusion flames. Combust Flame 1985;62:43–60. https://doi.org/10.1016/0010-2180(85)90092-6.

[50] Lee KB, Thring MW, Beér JM. On the rate of combustion of soot in a laminar soot flame. Combust Flame 1962;6:137–45. https://doi.org/10.1016/0010-2180(62)90082-2.

[51] Santoro RJ, Yeh TT, Horvath JJ, Semerjian HG. The Transport and Growth of Soot Particles in Laminar Diffusion Flames. Combust Sci Technol 1987;53:89–115. https://doi.org/10.1080/00102208708947022.

[52] Michelsen H a., Schulz C, Smallwood GJ, Will S. Laser-induced incandescence: Particulate diagnostics for combustion, atmospheric, and industrial applications. Prog Energy Combust Sci 2015:1–47. https://doi.org/10.1016/j.pecs.2015.07.001.

[53] Abboud J, Schobing J, Legros G, Matynia A, Bonnety J, Tschamber V, et al. Impacts of ester's carbon chain length and concentration on sooting propensities and soot oxidative reactivity: Application to Diesel and Biodiesel surrogates. Fuel 2018;222:586–98. https://doi.org/10.1016/j.fuel.2018.02.103.

[54] Braun-Unkhoff M, Riedel U. Alternative fuels in aviation. CEAS Aeronaut J 2014;6:83–93. https://doi.org/10.1007/s13272-014-0131-2.

[55] Lin H, Liu P, He Z, Zhang Y, Guan B, Huang Z. Formation of the first aromatic ring through the self-recombination of but-1-ene-3-yne with H-assistance in combustion. Int J Hydrogen Energy 2016;41:13736–46. https://doi.org/10.1016/j.ijhydene.2016.06.123.

[56] Liu P, Zhang Y, Wang L, Tian B, Guan B, Han D, et al. Chemical Mechanism of Exhaust Gas Recirculation on Polycyclic Aromatic Hydrocarbons Formation Based on Laser-Induced Fluorescence Measurement. Energy & Fuels 2018;32:7112–24. https://doi.org/10.1021/acs.energyfuels.8b00422.